Magnetorheological Fluids Subjected to Non-uniform Magnetic Fields: Experimental Characterization

Michal Kubík[1], Janusz Gołdasz[2]‡, Ondřej Macháček[1], Zbyněk Strecker[1] and Bogdan Sapiński[3]

[1]Faculty of Mechanical Engineering, Brno University of Technology, Technická 2896/2, Brno 61669, Czechia

[2] Faculty of Electrical and Computer Engineering, Cracow University of Technology, ul. Warszawska 24, 31-155 Kraków, Poland

[3]Department of Process Control, AGH University of Science and Technology, Al. Mickiewicza 30, 30-059 Krakow, Poland

E-mail: `janusz.goldasz@pk.edu.pl`

21 February 2024

Abstract.

Magnetorheological (MR) fluids are suspensions of fine, low-coercivity, high-magnetizable particles in a continuous liquid phase. When subjected to magnetic field, the material exhibits a rapid change in the apparent viscosity of several orders of magnitude. This unique capability has been successfully exploited in automotive semi-active suspensions systems or systems for manufacturing high quality optics. In a majority of the existing systems, the rheology of MR fluids is controlled by an external uniform field oriented perpendicularly to the fluid flow direction. In general, it is an inherent feature of MR systems operating in flow, shear or squeeze modes, respectively. There is an experimental evidence that the behavior of MR fluids in

‡ Corresponding author

the so-called pinch-mode (in which the fluid is subjected to non-uniform magnetic field distributions) clearly stands out against the remaining three operating modes. With the predecessors, the flow through the channel occurs once a pressure across it exceeds the field-dependent threshold pressure. For comparison, in pinch mode valves the magnetic flux energizes mostly the layers of the materials near the channel walls. The outcome is a change in the channel's effective diameter achieved solely via material means without changing its geometry. To study the fluid's unique behaviour in the pinch mode, the authors designed a prototype valve assembly and examined several fluid formulations of various particle concentration levels across a wide range of external (velocity, magnetic field density) stimuli in an organized effort to further comprehend the phenomenon. The obtained data indicate that the magnitude of the particular effect does not only depend on the magnitudes of the magnetic stimuli but also on the particle concentration; the smaller the concentration of particles the more pronounced the pitch mode like behavior is. In general, the authors believe that the study may provide guidelines as to the selection of fluid formulations for developing novel valveless actuators utilizing MR fluids operating in pinch mode.

Keywords: magnetorheological fluid, operating mode, pinch mode, magnetic field, valve

1. Introduction

To begin with, magnetorheological (MR) fluids are suspensions of fine, low-coercivity, high-magnetizable particles in a continuous liquid phase. These micron-size particles are usually made of carbonyl iron powder (CIP). The liquid phase of MR fluids (carrier oil) has been typically based on silicon or synthetic hydrocarbon oils [1]. The carrier fluid is chemically compatible with the particles, exhibits low thermal expansion, excellent lubricity, acceptable viscosity across a wide operating temperature range. Moreover, specific additives affect the rheological [2, 3] or tribological [4, 5] properties of MR fluids as well as improve their sedimentation stability [6, 7]. In the presence of magnetic field the ferromagnetic particles in the fluid are magnetized and form chain-like structures along the magnetic flux lines, thus resisting the fluid flow. As a result, the MR fluid exhibits a rapid change in the apparent viscosity of several orders of magnitude [8].

By principle, MR fluids' unique characteristics can be best exploited in various fundamental modes, i.e. (i) flow-mode, (ii) shear-mode, (iii) squeeze-mode or (iv) (gradient) pinch mode. In (i) flow mode, the fluid flows between two stationary (planar or annular) surfaces due to a pressure gradient. The rheology of the material is controlled by an external magnetic field oriented perpendicularly to the fluid flow direction. In flow-mode hardware the distribution of magnetic field in the channel (air gap) is usually homogenous. This mode is typical for linear long-stroke MR dampers [9, 10, 11], and has been commercialized, e.g. in automotive suspension dampers, powertrain mounts [12, 13] in passenger vehicles or seismic dampers [14]. For comparison, in (ii) shear mode, the fluid flows between two surfaces moving relatively against each other. Similarly to flow mode devices, the magnetic field in shear-mode hardware is oriented perpendicularly to the fluid flow direction and efforts are made to ensure the field distribution is homogenous. Exemplary devices include rotary dampers [15], clutches [16] or brakes [17]. Next, in (iii) squeeze mode, the fluid is compressed between two planar parallel surfaces. In this configuration the height of the flow channel is varied according to the prescribed displacement or force. Exemplary devices include small stroke dampers [18] or engine mounts [19] in which a rather large force can be achieved across a fairly small displacement span. The (iv) pinch mode principle is different. While in the previous modes the field distribution is usually homogenous, and the flux crosses the flow channel in the direction perpendicular to the fluid flow, in pinch mode the flux path is directed in such a way so as to possibly energize only the layers of fluid in the areas adjacent to the walls (ideal scenario). With the material solidified locally in the near-wall regions the configuration can be compared to that of a valveless controlled orifice. In this case the magnetic field distribution is non-uniform. As it seems, the mechanisms governing the behaviour of MR fluids subjected to non-uniform magnetic fields have been studied and researched to a far lesser extent than the predecessors.

So far, only a handful of publications have dealt with the rheology of MR fluids in pinch mode. In 2008, Carlson et al. [20] patented an MR valve operating in pinch mode. In the patent application the researchers described a method of varying the effective diameter of a flow channel with a non-uniform magnetic field distribution in addition to providing several arrangements of the magnetic circuit. Next, Goncalves and Carlson [21] highlighted the results of a rudimentary experimental study on the pinch mode valve concept in an attempt to prove the principle. Recently, Lee et al. [22] developed a simplified mathematical model for studying the flow of MR fluids subjected to non-uniform magnetic fields. The model was verified against experimental data across a specified magnetic field strength variation range (as well as the flow rate). Also, Gołdasz and Sapiński [23] carried out a magnetostatic analysis of a pinch MR valve. The researchers tested several fundamental configurations of the solenoid and examined their magnetic characteristics through magnetostatic finite element (FE) analyses. Moreover, the CFD study of Goldasz et al. [24] revealed the theoretical relationships between the pressure drop across the flow channel and the average flow velocity. The study utilized several pinch valve configurations having at least one energized MR fluid zone in the channel or several zones in series. Finally, Kubík et al. [25] proposed an MR fluid shaft seal. In the examined seal assembly the fluid is energized in a manner similar to that of pinch mode.

The behavior of the fluid in pinch mode is clearly different than in the other three fundamental operating modes. For instance, in flow mode valves, the flow through the valve occurs only upon exceeding the magnetic field-dependent threshold pressure. That is the result of magnetic flux crossing the entire gap and energizing the entire fluid volume. For comparison, in pinch mode valves the flux travels along the flow channel between the neighbouring poles. As a result, only near-the-wall fluid layers are energized. The effect is the change of the effective diameter of the flow channel. Thus, the Venturi-type effect is achieved solely by material means rather than modifications of the geometry of the flow path as in modern state-of-the-art controlled solenoid valves. As mentioned, the principle was experimentally demonstrated by Goncalves and Carlson [21] or Lee et al. [22]. However, their experimental verification was based on several discrete measurement points; the valve's behavior between those points or beyond them is unknown. Also, the details of the Goncalves' study were not revealed by the authors. Moreover, Xuan et al. [26] suggested that the shear stress and the microstructure of MR fluids subjected to non-uniform magnetic fields are very different from the uniform magnetic field scenarios. In addition to that, the number of tested MR fluid formulations (and thus the range of material properties) was limited (Lee et al. – fluid: MRF-132DG, Goncalves et al. – fluid: several unknown formulations). For instance, the effects of MR fluid composition (particle concentration, MR fluid type, etc.) on the pinch mode valve performance and limits were not evaluated yet.

It is then the intent of the authors to fulfill the gap. Thus, in this paper the authors reveal the results of an experimental study involving several fluid formulations subjected to a range of hydraulic and magnetic stimuli. In brief, Section 2 reveals the pinch mode fundamentals. In Section 3 the authors presents the pinch mode valve prototype concept complemented by its extensive magnetic analyses. Next, Section 4 highlights the experimental test rig setup, reveals the material data as well as the assumed range of magnetic fields and the input flow rates. The section is complemented by the experimental results. Section 5 provides a discussion on the study's outcome, and conclusions are provided in Section 6.

2. Principle of MR fluids behaviour in pinch mode

The flow of MR fluids in pinch mode is a pressure-driven flow as in flow (valve) mode. However, the fundamental difference between them is in the distribution of magnetic field in relation to the fluid flow (and thus the design of magnetic circuits). As already mentioned, in flow mode the flux passes the flow path (air gap) perpendicularly to the fluid flow direction as in Figure 1(a), whereas in pinch mode the flux passes from one pole to another without energizing the entire fluid volume in the channel. As simply shown in Figure 1(b) this configuration results in a highly non-uniform magnetic field, and the flux travels along the pinch gap from one magnetic pole to the other. The flux's shortest path is close to the channel's wall. As the reluctance increases with the distance to the center of the pseudo-orifice the lowest magnetic flux density is at center of the orifice. That is clearly different than in the remaining three operating modes as mentioned above. From the microscopic point of view, the iron particles would form chains (clusters) in the direction of the magnetic field, and the magnetic forces between them would be stronger near the pseudo-orifice's wall than at the center – see Figure 1(b). Thus, the MR fluid flow can be initiated in the areas in which the pressure drop $\Delta p = p_1 - p_2$ exceeds the local threshold pressure due to the activated yield stress change. This is a fundamental principle of an MR fluid pinch valve in which the effective diameter of the orifice D_{eff} can be controlled by the magnetic field. The change in the magnetic field level results in variations of the effective diameter and the

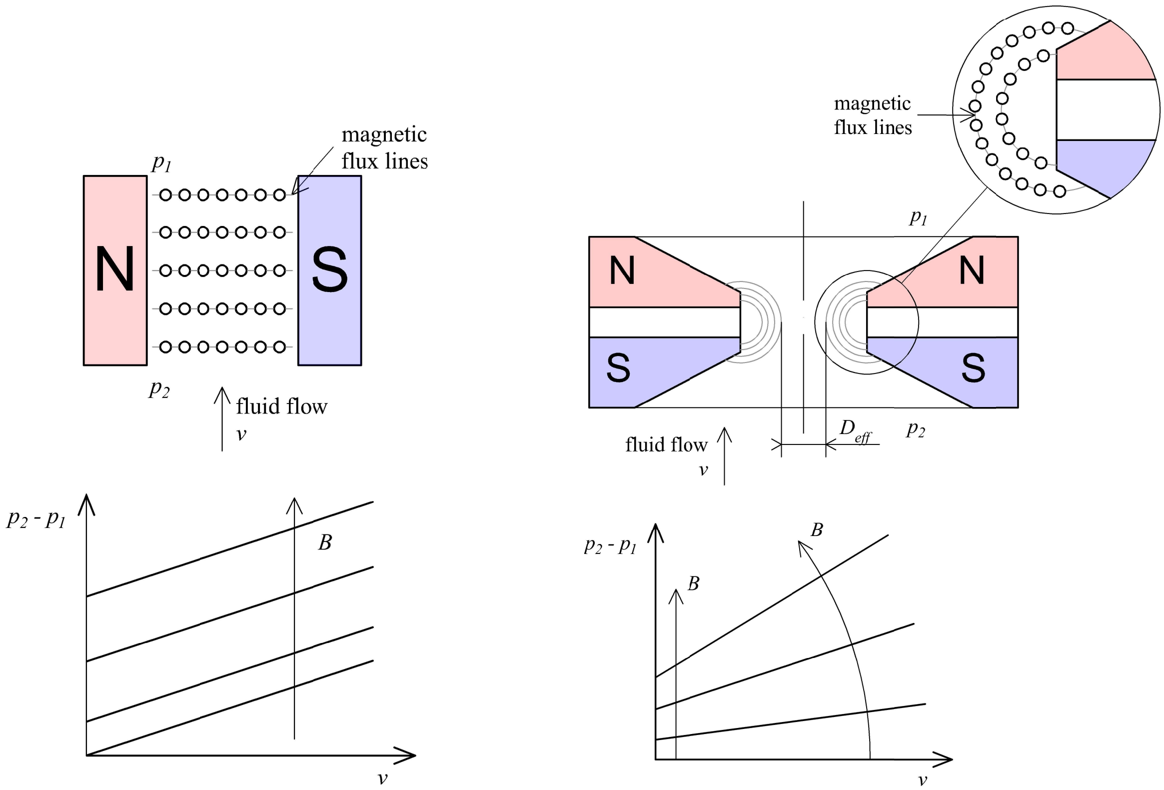

(a) flow-mode principle [27] (b) gradient pinch mode concept [21]

Figure 1. Conceptual MR valves and flow characteristics: flow mode valve (a); pinch mode (b)

fluid's velocity v. Note that it is a significant simplification of the behavior of MR fluids in pinch mode, and the exact behavior will need to be described using numerical models, model-based visualizations or experiments. Goncalves and Carlson [21] suggested that the rudimentary Wuest equation for describing the fluid flow through a sharp orifice can be used to estimate the effective orifice diameter in the following form

$$\Delta p = \frac{50.4\eta Q}{\pi D_{eff}(B)^3} \tag{1}$$

where η – MR fluid viscosity, Q – volumetric flow rate, Δp – pressure drop, and B – magnetic flux density, D_{eff} – effective diameter. It needs to be noted that in addition to the $\Delta p - Q$ characteristics slope variations, the pinch valve also exhibits a change in the pressure offset due to the non-zero magnetic field in the center of the orifice. It is inline with regular flow-mode valves, however, the slope change feature is a unique feature of pinch mode valves.

3. MR pinch valve prototype

To study the MR fluid behaviour the authors developed a single-gap MR pinch mode valve concept. The examined MR pinch valve assembly incorporates the thru-hole channel (1), the magnetic core assembly (2), the control coil (3), and the MR fluid (7) – see Figure 2. In the fabricated prototype the diameter of the thru-hole was $D = 3$ mm and its length was equal to $L_g = 30$ mm. The distance between the magnetic poles was $w = 1$ mm. The core assembly reveals two magnetic pole pieces (4), the bronze non-magnetic spacer (5), and the air gap (6). The purpose of the air gap (size – 0.8 mm) was monitoring the flux in the magnetic circuit with the Hall probe. The core was manufactured out of low-carbon 11SMn30 steel. The electromagnetic coil incorporates $N = 300$ wire turns (wire diameter – 0.6 mm) wounded on to an aluminum carcass.

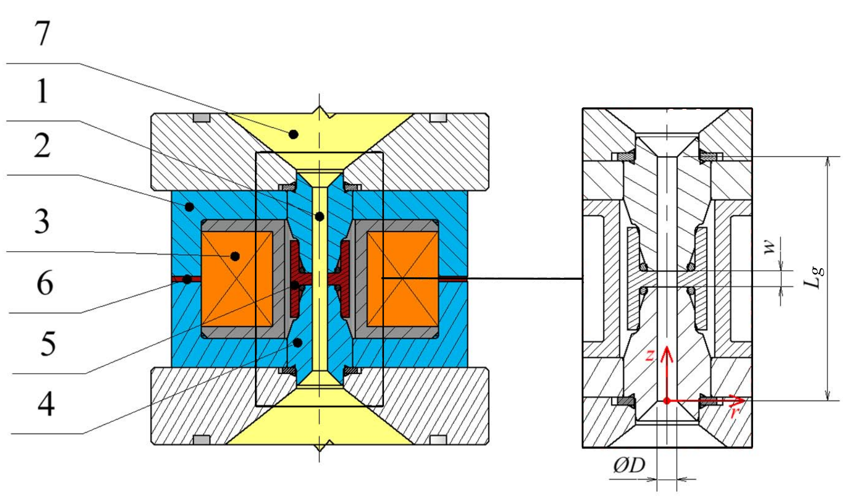

Figure 2. Magnetic pinch valve; low-carbon steel (blue), MR fluid (yellow), aluminum (grey), bronze (red), copper (orange)

Sizing the valve assembly was based on the outcome of the magnetostatic analysis.

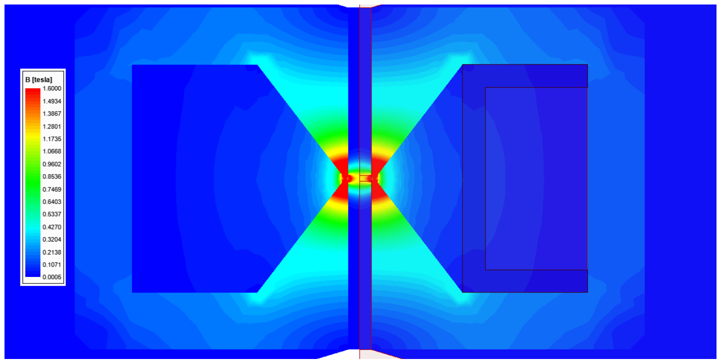

Figure 3. Flux density distribution in the solenoid valve assembly; $NI = 1200$ A, $D = 3$ mm

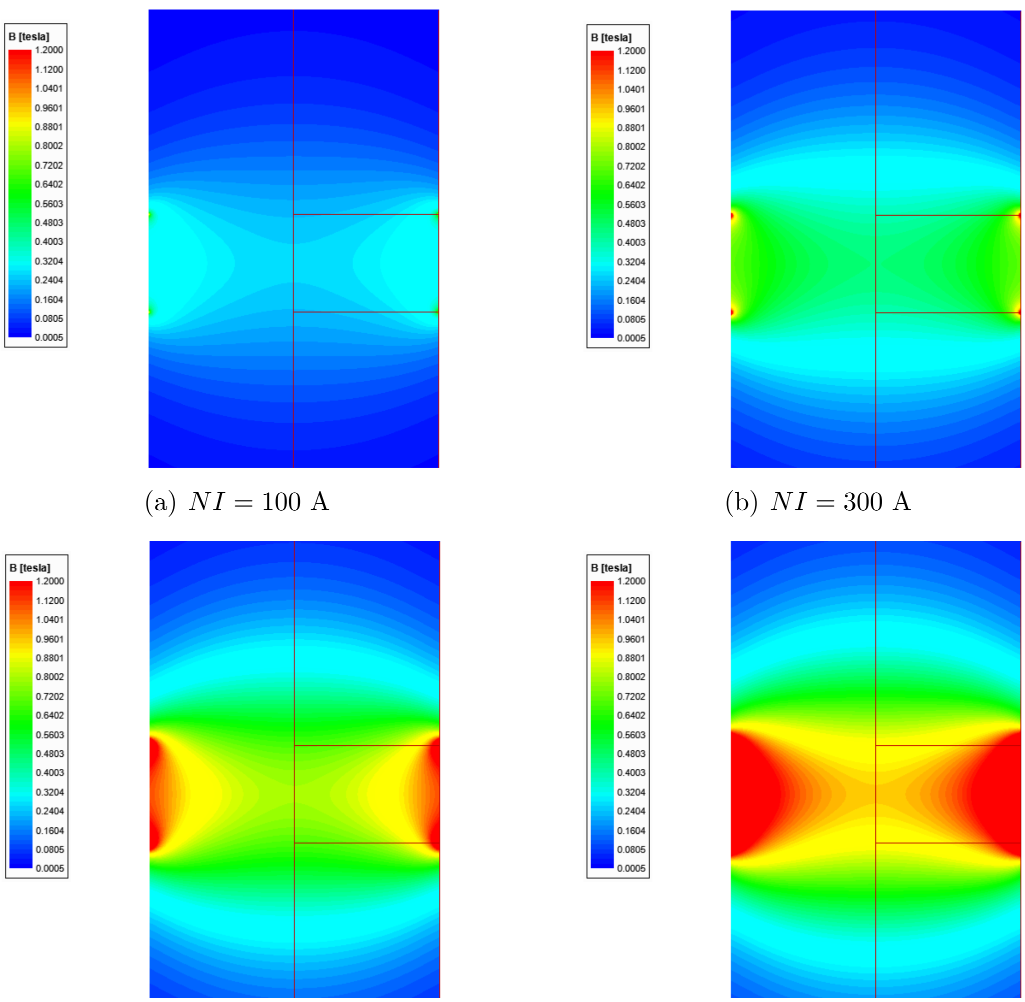

(a) $NI = 100$ A

(b) $NI = 300$ A

(c) $NI = 600$ A

(d) $NI = 900$ A

Figure 4. Flux density distribution in the pinch gap, $D = 3$ mm

The geometry presented in Figure 2 was modeled in Ansys Maxwell R2021. The purpose of this exercise was to evaluate the steady-state performance of the EM circuit and to

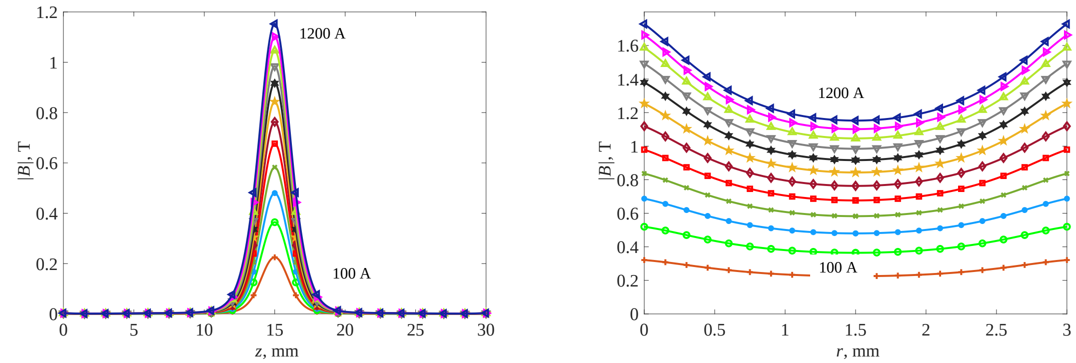

(a) $|B| - z$ (b) $|B| - r$

Figure 5. Variation of flux density in the pinch gap

identify potential flaws or bottlenecks in the assembly. The magnetostatic analysis was performed within the ampere turns range NI from 100 to 1200 A. The MR fluid $B - H$ magnetisation curve was that of a typical 22 % Fe vol. The exemplary results are illustrated in Figures 3 to 5. In particular, Figure 3 reveals the flux density distribution in the assembly at 1200 A. In the presented example the flux's largest concentration in the area between the adjacent poles is evident. The observation is reinforced by analyzing the zoomed-in data in Figure 4. It can be seen that as the input current amplitude (ampere turns) increases the gap flux density is altered accordingly, however, the largest local values of the flux density vector can be noticed in the areas near the walls. The flux density maps also make it clear that the smallest values of B are at the center of the thru-hole in between the neighboring poles. Furthermore, Figure 5(a) highlights the variation of the gap flux density along the gap length and at the thru-hole centerline, whereas Figure 5(b) shows the flux density transition between the channel wall and the centerline. The results confirm that the largest concentration of flux is in the region above the non-magnetic spacer separating the poles. Also, it becomes evident that at the ampere turns the flux density is almost invariant of the distance from the hole's wall. As the ampere turns increase the difference between the flux density value at the wall and the flux density at the center of the gap becomes significant. This is likely due to the saturation of the magnetic poles and the resulting flux leakage (bypassing the flow path). Based on the observations of Figures 5(a) and 5(b) the usable operating range of the solenoid valve was determined to be 0-900 A (ampere turns).

4. Testing of MR fluids in pinch mode

The section highlights the test rig and the setup. That is followed by a brief description of the test inputs and the test scenarious as well as a summary of the properties of the MR fluids used during the experiments. The section is complemented by a presentation of the obtained experimental results.

4.1. Test rig

The layout of the test rig is simply shown in Figure 6(a). The flow of MR fluid is imposed by the Inova hydraulic dynamometer AH 40-150 which imposes the motion of the floating piston (D_p=32 mm, D_p – piston diameter) through the flow channel in the slit-gap rheometer. The top & bottom pistons are connected by a rigid frame. The pressure drop across the valve was monitored with two pressure sensors of the type HBM P8AP (10 bar). The MR fluid temperature was acquired using the sensor PT100 located near the entrance to the MR pinch valve (pinch gap). The position of the floating piston was measured by the Megatron resistance position sensor RC13. The magnetic flux density in the air gap was measured using the fluxmeter Bell 5180 with the ultra-thin transverse probe STB1X-0201. The Fluke i30 current clamp was used to monitor the electric current supplied to the coil. The voltage at the coil terminals was measured directly. The signals were recorded at the sampling frequency of 1 kHz with the data analyzer Dewe-800.

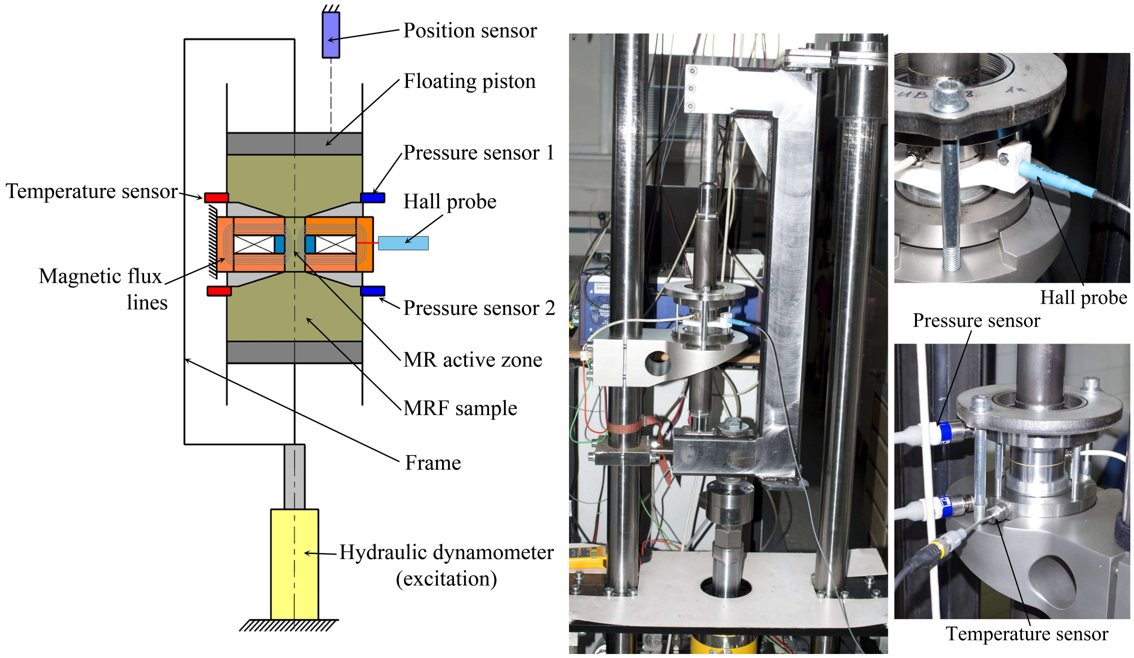

(a) rig layout (b) actual setup

Figure 6. Test rig: layout (left); photo (right)

4.2. Test scenarios and material data

During the flow measurements all data were acquired using the constant acceleration displacement profile imposed by the Inova stroker – see Figure 7. Therefore, the input velocity was linearly increasing and decreasing in the same fashion. This method of excitation was chosen as the most convenient upon preliminary testing. The data were subsequently filtered in the post-processing stage; a 50-sample moving average filter was applied to the measured data. The fluid flow velocity in the channel was calculated on the basis of the continuity equation and the measured piston velocity; given the diameter of the thru-hole the calculated hydraulic ratio is equal to $(D_p/D)^2 = 113.8$. The velocity (flow rate) excitation range is from 0 to 0.96 l/min (16000 mm^3/s). The MR fluids used in the tests are listed in Table 1. The key differences are in the iron (solid phase) content (as well as the resulting base viscosities). Note that difference between MRF-122EG and MRF-140CG is nearly twice the iron content (22% vs 40%)

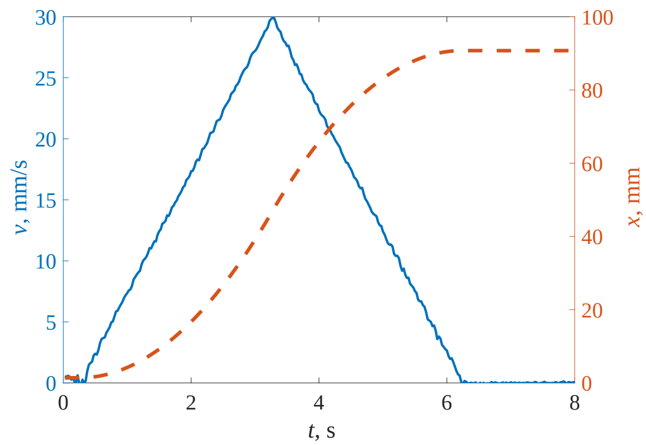

Figure 7. Input excitation waveform $-x(t)$ & $v(t)$

Table 1. Tested MR fluids

	Fe vol, %	Base viscosity μ at 30^{o}C, cP
MRF-122EG	22	56
MRF-132DG	32	156
MRF-140CG	40	648

which translates into significant differences in the key material properties. During the experiments each fluid sample was subject to identical series of tests for the ease of comparison.

4.3. Results

Effect of magnetic field To begin with the MRF-122EG reference fluid, Figure 8(a) shows the MR valve pressure drop versus flow rate data collected during the velocity increase stage and the velocity decrease stage, respectively. The illustration shows the data at various levels of the magnetic flux density (or ampere turns up to 900 A). The measured data were curve-fitted using linear regression. In Figure 8(a) the increase in the slope of the flow curve and the offset change with the increase in the magnetic field are evident. In addition to that in Figures 8(c) and 8(d) the pressure and flow rate data were non-dimensionalized and plotted in terms of the friction factor C_f vs Reynolds number Re. The dimensionless numbers were calculated as follows

$$Re = \frac{\rho \bar{v} D}{\mu} \quad C_f = \frac{2D\Delta p}{L_g \rho \bar{v}^2} \tag{2}$$

where $\bar{v}$ – fluid's mean velocity in the channel.

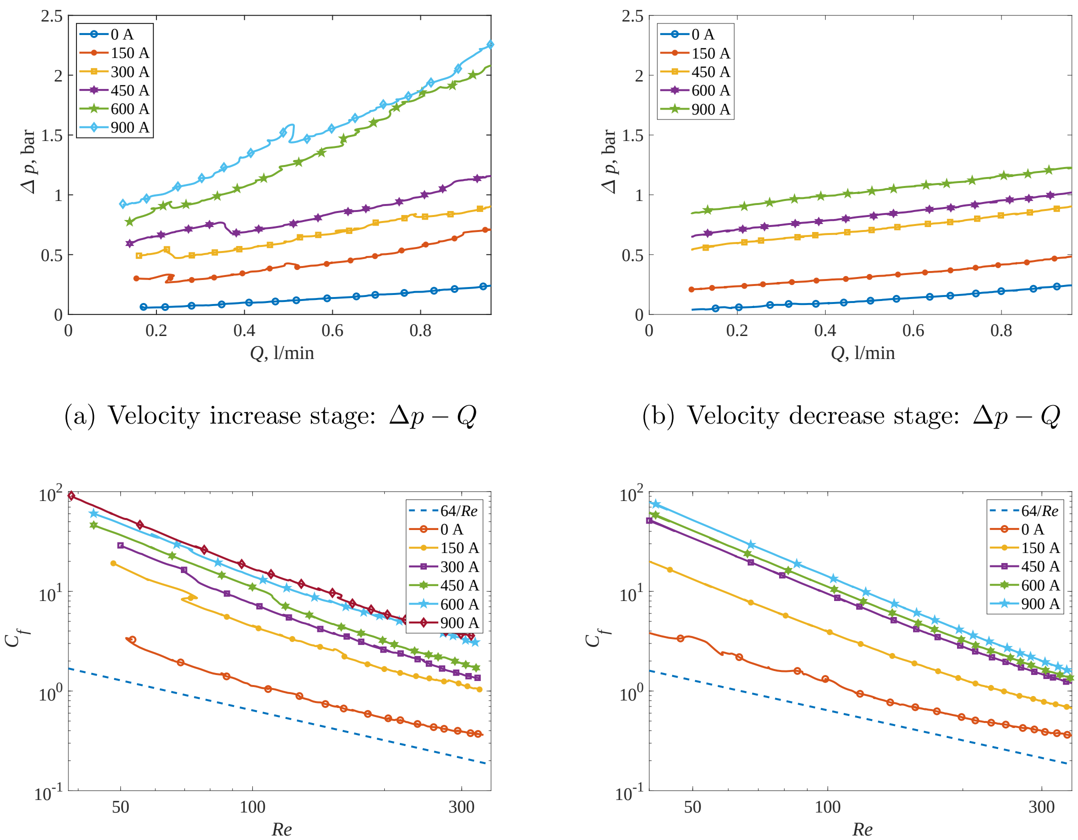

(a) Velocity increase stage: $\Delta p - Q$

(b) Velocity decrease stage: $\Delta p - Q$

(c) Velocity increase stage: $C_f - Re$

(d) Velocity decrease stage: $C_f - Re$

Figure 8. MRF-122EG results: flow characteristics

To estimate the pressure-flow rate curve slope variation the authors introduced the two additional parameters: $k(B)$ – the pressure-flow rate curve slope at a given magnetic flux density level (or the current I), $K = k(B)/k(0)$ – dimensionless slope factor. The parameter k can be deduced via linear regression. As calculated from the measured data, the estimated pressure-flow rate characteristics slope varies by a factor of $K = 6.6$ at the maximum ampere turns level of 900 A when compared to the base (off-state) curve at 0 A – see Table 2. The temperature was maintained at 30^{o}C during the experiments.

This is inline with the experiment of Goncalves and Carlson [21] ($K = 6$ est.). It should be noted, however, that only the off-state pressure-flow rate curve slope is nearly the same for either stage of the velocity input change. The situation is significantly different with the energized scenarios. In the velocity decrease stage the slope change is significantly lower than in the velocity increase portion of the excitation profile – the latter contributing to $K = 1.7$ as also revealed in Table 2 and Figure 8(b). Moreover, this change is almost independent of the magnetic field. In this excitation mode, the valve behaves in a manner typical to common flow-mode MR valves, where the pressure offset increases with the increasing magnetic flux density (material's yield stress). Another significant difference between these excitation modes is the smoothness of the flow curve with respect to both stages of the input velocity profile. The obtained data reveal that during the velocity increase stage the pressure-velocity on-state curves reveal pressure pulsations; the mechanism behind the phenomenon is discussed in Section 5. Finally, it should be noted that the $C_f - Re$ off-state (0 A) characteristics deviate from the theoretical solution. It is likely due to the fluid's off-state (low but finite) yield stress.

Table 2. MRF-122EG: slope variation with current, R – norm of residuals

Ampere turns, A	k, bar·min/l	K	Offset, bar	R^2
Velocity increase stage				
900	1.60	6.60	0.66	0.98
600	1.63	6.71	0.48	0.98
300	0.55	2.27	0.36	0.97
0	0.24	1.00	0	0.98
Velocity decrease stage				
900	0.42	1.74	0.81	0.99
600	0.41	1.69	0.62	0.99
300	–	–	–	–
0	0.24	1.00	0	0.98

Next, Figure 9 shows the repeatability of the measurement at $NI = 900$ A and during both stage of the excitation profile. It is evident that the repeatability is rather poor – the measured data show abrupt pressure variations. The largest recorded pressure drop of 0.54 bar was measured during the third consecutive run. This behavior occurs at various gap velocities for the same excitation condition (ampere turns level) as seen in Figure 9. The magnitude of the pressure variations is not constant but depends on the

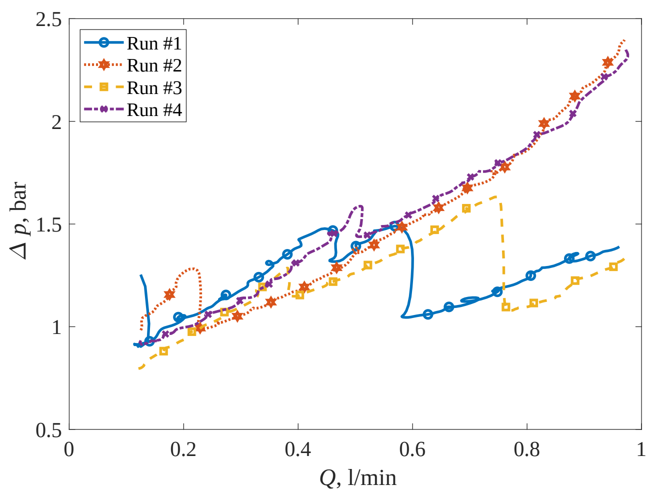

Figure 9. MRF-122EG: repeatability of the experiments, $NI = 900$ A

magnetic field level. Its magnitude decreases with the decreasing magnetic field. Aside from the pressure oscillations, the experiment repeatability is acceptable. Rodriguez et al. [28] observed a similar trend curve as in the present study. The authors stated that the non-monotonic shape of these curves could be explained in terms of the competition between the two opposite effects: (i)) an increase of the hydrodynamic dissipation and (ii) weakening of the interaction between aggregates and walls during the suspension flow velocity increase.

To further investigate the phenomenon, both the magnetic flux density in the air gap and the coil voltage were monitored during the experiments. As an example, Figure 10(a) shows the time histories of pressure drop across the valve and the magnetic flux density in the air gap. It is evident here that the change in the pressure drop is

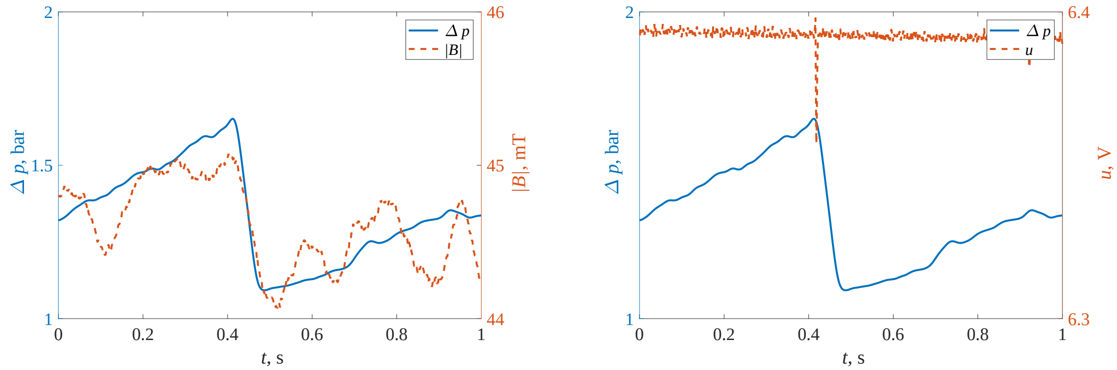

(a) $\Delta p - t$, $|B| - t$

(b) $\Delta p - t$, $u - t$

Figure 10. MRF-122EG: time histories of pressure, flux density and voltage

accompanied by variations of the magnetic flux density in the air gap. The flux density change is relatively small (2.3 %) but measurable and evident. The same observation can be applied to the coil voltage as shown in Figure 10(b). Note that the induced voltage e is related to the magnetic flux ϕ; $e = -N\dfrac{d\phi}{dt}$. The magnetic flux change can be caused either by a change in the relative permeability of a component of the magnetic circuit or by pulsations in the power supply. The coil power supply was positively tested and its malfunctions were ruled out. Therefore, it is likely that this behavior is due to variations of the permeability of the MR fluid sample. On the particle level, if a significant portion of a cluster of particles is pushed out of the energized zone; the concentration of the particles in the zone decreases at a given time, and the permeability of the fluid varies. The finding can be reinforced by observations of the data in [20] where similar effects can be seen.

Effect of particle concentration This section reveals the results obtained with the other two fluids (MRF-132DG & MRF-140CG) in an effort to examine the effect of particle concentration (and the resulting contribution of yield stress). Figure 11(a) shows the relationship between the pressure drop across the valve and the flow rate for MRF-

132DG fluid sample measured during the velocity increase stage of the input excitation; the fluid's iron content is 32% as opposed to the previously tested 22% sample (MRF-122EG). In this case the slope factor K was determined to be equal to 2.76 – see Table 3. When compared to the MRF122EG sample, the gain is significantly smaller, although the increase in the slope and the pressure offset in the pressure drop-velocity characteristics following the magnetic field change are evident. During the velocity decrease stage the change in slope is relatively small and almost independent of the magnetic field magnitude as seen in Figure 11(b) and Table 3. The same fluid was used by Lee et al. [22] in their pinch mode experiments, and the slope factor was determined to be $K = 17$ (est.). That value is significantly higher than in the present study.

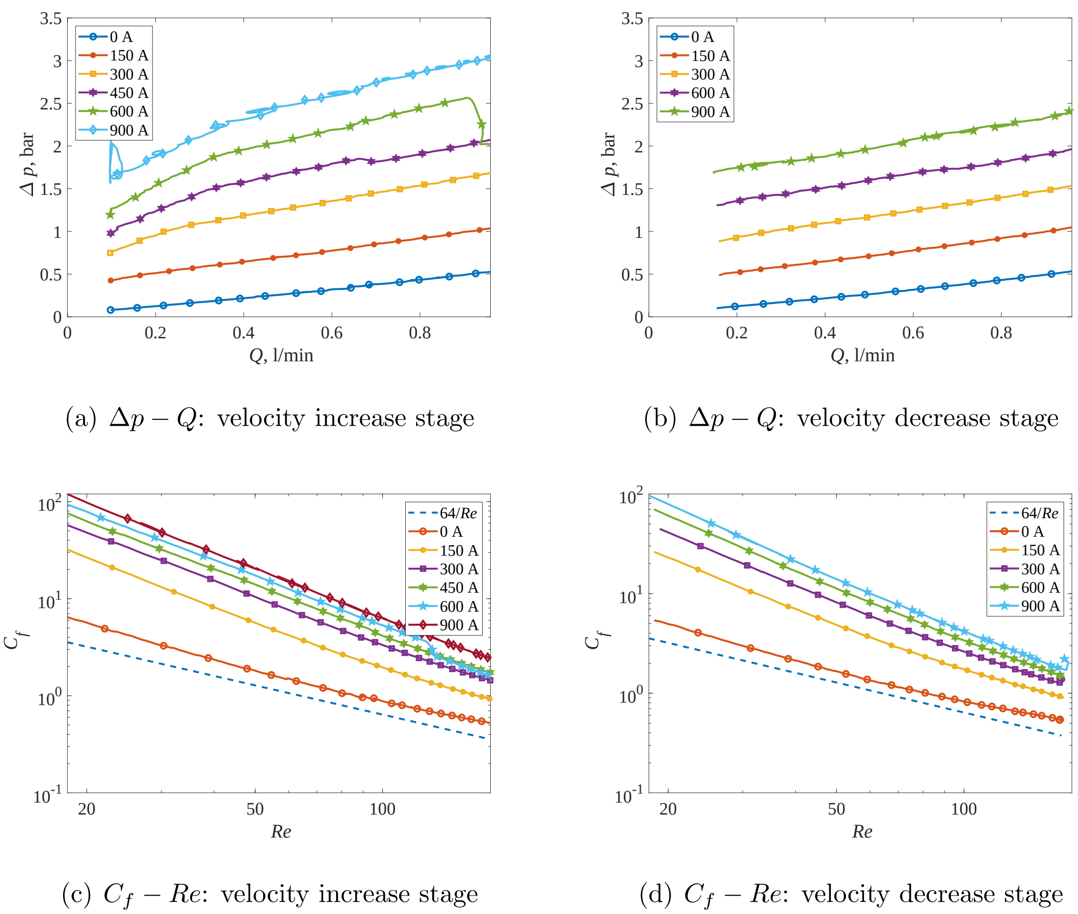

(a) $\Delta p - Q$: velocity increase stage

(b) $\Delta p - Q$: velocity decrease stage

(c) $C_f - Re$: velocity increase stage

(d) $C_f - Re$: velocity decrease stage

Figure 11. MRF-132DG: flow characteristics

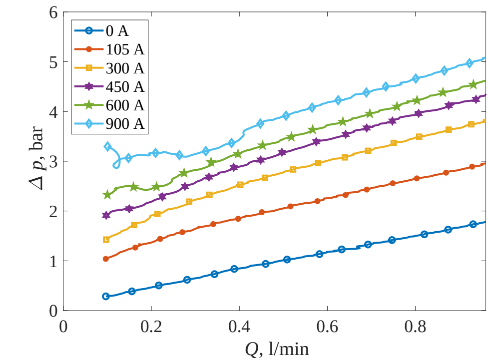

(a) $\Delta p - Q$: velocity increase stage

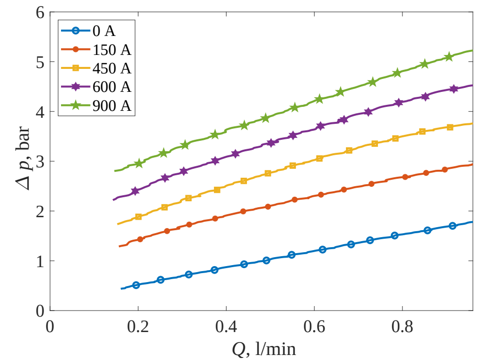

(b) $\Delta p - Q$: velocity decrease stage

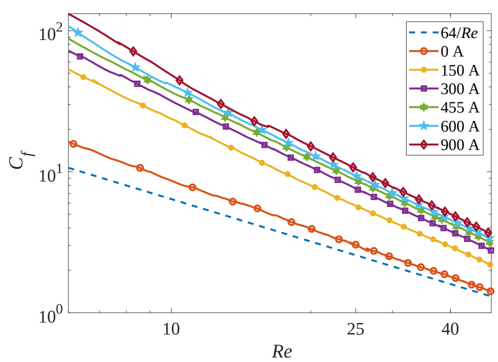

(c) $C_f - Re$: velocity increase stage

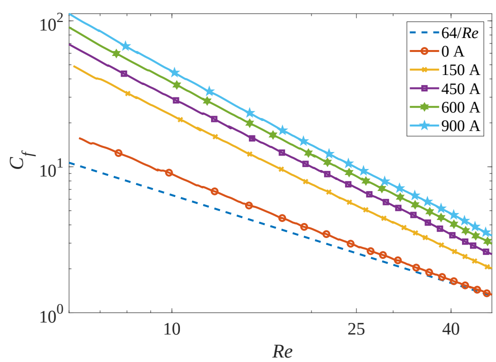

(d) $C_f - Re$: velocity decrease stage

Figure 12. MRF-140CG: flow characteristics

Table 3. MRF-132DG: slope variation with current

Ampere turns, A	k, bar·min/l	K	Offset, bar	R^2
Velocity increase stage				
900	1.50	2.76	1.65	0.97
600	1.43	2.64	1.31	0.97
300	0.95	1.75	0.78	0.99
0	0.54	1.00	0	0.99
Velocity decrease stage				
900	0.85	1.58	1.55	0.99
600	0.78	1.45	1.20	0.99
300	0.79	1.46	0.77	0.99
0	0.54	1.00	0	0.99

Table 4. MRF-140CG: slope variation with current

Ampere turns, A	k, bar·min/l	K	Offset, bar	R^2
Velocity increase stage				
900	2.62	1.54	2.54	0.98
600	2.74	1.61	2.03	0.99
300	2.59	1.53	1.40	0.99
0	1.71	1.00	0	0.99
Velocity decrease stage				
900	3.00	1.81	2.37	0.98
600	2.84	1.71	1.90	0.99
300	2.59	1.56	1.41	0.99
0	1.66	1.00	0	0.99

Moreover, Figure 12 reveals the measurements obtained with the MRF-140CG fluid sample. As seen in Figure 12(a), the slope factor is degraded to $K = 1.54$ as highlighted in Table 4. However, the pressure variations which were observed with the previously tested fluid samples almost completely disappeared in the case of the MRF-140CG sample. The change in slope is the same for either stage of the excitation – see Figure 12(b) and Table 4. Also, note that the base $\Delta p - Q$ curve shows an offset, which is likely to be due to the material's off-state (small yet finite) yield stress and the contribution of the flow losses at the entry/exit to channel.

5. Discussion

The following section summarizes the crucial results of the experiments. The authors made an attempt to analyze them, and describe or propose the possible mechanisms or explanations contributing to the observed behaviors. Based on the analysis of the obtained data the authors conclude that

i The slope factor K value is higher for the low Fe concentration samples.

ii The slope change in the pressure-velocity characteristics is significantly less pronounced during the velocity decrease stage.

iii Pressure pulsations occur during the experiments. They are accompanied by simultaneous changes in the magnetic flux and the induced coil voltage, respectively.

iv As the particle concentration increases, the observed pressure pulsations disappear and the slope changes are significantly lower. There is no change in the slope factor value in either stage of the input excitation.

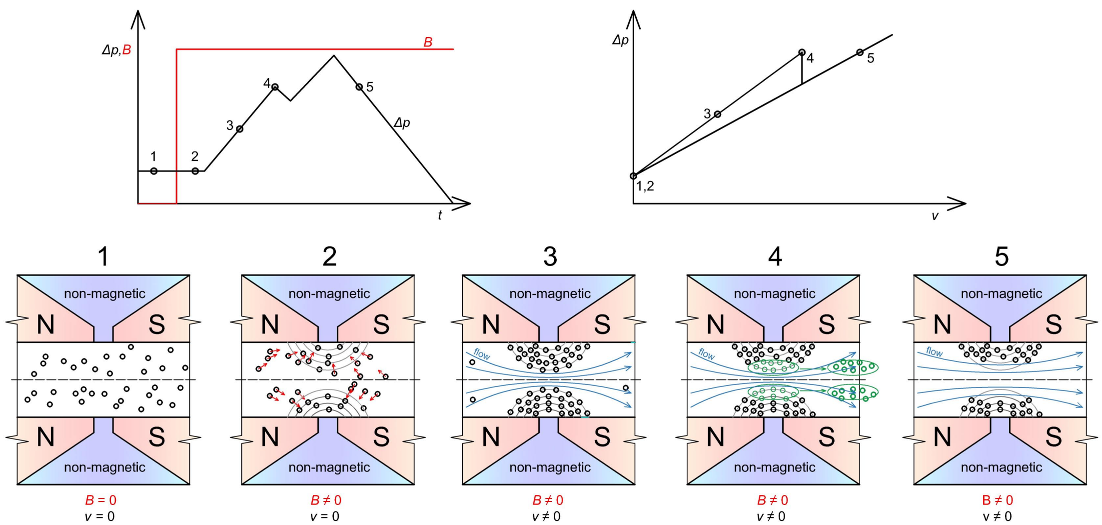

Figure 13. Description of the pinch mechanism

As way of explanation, it is likely that the ferromagnetic particles migrate to the high flux density regions as simply shown in Figure 13 (see the illustration no. 2). This migration is caused by the Kelvin force (also known as the magnetic field-gradient force or magnetophoretic force) [29, 30]. Therefore, the particle concentration is likely to increase in this region (active zone) up to the particle packaging limit. This particle packaging limit is likely to be similar for the two fluid samples: MR-122DG and MRF-132DG. That is why the slopes in the pressure-velocity characteristics of these two fluids are quite similar (in absolute terms). Increasing the concentration of particles follows the increase in the relative permeability of the MR fluid in the active (energized) zone.

As soon as a significant volume of the particle clusters is forced out of the active zone due to a pressure drop, it has to develop an instantaneous pressure drop change and changes in the magnetic flux in the circuit (magnetic reluctance) as highlighted in Figure 13 (see the illustration no. 4). This behavior can be related to the observations (i) and (iii). In the velocity decrease stage, the particles do not have the time to move to the active zone (with the higher magnetic flux density) as they are simply washed out due to the fluid flow. Therefore, there is no increase in the particle concentration level and thus the curve slope changes only a little. This corresponds to the observation (ii). This was also observed in our experiment during which the magnetic field was switched on in the velocity increase stage and not before the measurement start. In this case, the slope change was not significant. Finally, in the MRF-140CG case, the particle packaging is so high that the particle concentration cannot be increased in the active zone. Thus, a significant change in slope does not occur. This corresponds to the comment (iv).

Perhaps, a better insight into the phenomenon can be provided with macroscopic multiphysics coupled magnetic and CFD simulations of MR fluid flows or multi-scale model for analyzing the motion of individual particles in high flux density zones.

6. Conclusions

In the essence, the purpose of the present (mostly experimental) study was to examine the behaviour of MR fluids under to non-uniform magnetic fields. The operation regime is unique for the material and provides distinctive flow characteristics which makes it stand out against the other operating modes. First, a prototype MR pinch mode valve assembly was developed, modeled and characterized. Second, several fluid formulations were tested using the developed pinch-mode valve concept to analyze their pinch-mode performance. Particularly, the impact of magnetic field and various particle concentrations were investigated, respectively. To the best knowledge of the authors, it is the first published attempt to characterize the pinch mode behaviour of MR fluids in such terms and conditions. The variety of selected fluid samples allowed to analyze their behaviour within a wide range of material properties from a low particle concentration fluid up to a MR formulation having a near-packaging limit particle concentration level.

The results revealed that although the magnetic field affects both the slope and the threshold (offset) pressure, the magnitude of the effect (slope change with magnetic field) varies among the tested samples. In general, the determined slope factor decreases with the increase in the particle concentration. Moreover, it is evident that the flow velocity change rate has a noticeable impact on the slope factor.

In general, the authors conclude that further studies are required on the subject. Modeling flow of MR fluids in this particular operation regime may provide a better in-depth explanation of the observed behaviours and is planned to complete in the following stage of the present project.

Acknowledgments

The first, third and fourth author wish to acknowledge the kind support of the Czech Science Foundation (Grantová Agentura České Republiky - GACR) – grant ID: GACR 21-45236L. The second and fifth authors acknowledge the support of the National Science Centre (Narodowe Centrum Nauki - NCN, Poland) – grant ID: 2020/39/I/ST8/02916.

References

[1] Y Zhang, J Jiang, Ch Ouyang, Y Meng, W Jia, L Ma, and Y Tian. Effect of base oil lubrication properties on magnetorheological fluids. *Smart Materials and Structures*, 30(9):095011, 2021.

[2] X Zhang, X Liu, J Ruan, Xand Zhao, and X Gong. The influence of additives on the rheological and sedimentary properties of magnetorheological fluid. *Frontiers in Materials*, 7:631069, 2021.

[3] JQ Zhang, J Zhang, and Q Jing. Effect of seven different additives on the properties of MR fluids. In *Journal of Physics: Conference Series*, volume 149, page 012086. IOP Publishing, 2009.

[4] S Kumar, R Sehgal, MF Wani, and MD Sharma. Stabilization and tribological properties of magnetorheological (MR) fluids: A review. *Journal of Magnetism and Magnetic Materials*, 538:168295, 2021.

[5] J Roupec, F Jeniš, Z Strecker, M Kubík, and O Macháček. Stribeck curve of magnetorheological fluid within pin-on-disc configuration: an experimental investigation. *Materials*, 13(20):4670, 2020.

[6] J Roupec, L Michal, Z Strecker, M Kubík, O Macháček, and HJ Choi. Influence of clay-based additive on sedimentation stability of magnetorheological fluid. *Smart Materials and Structures*, 30(2):027001, 2021.

[7] A Ronzova and M Sedlacik, Mand Cvek. Magnetorheological fluids based on core–shell carbonyl iron particles modified by various organosilanes: synthesis, stability and performance. *Soft Matter*, 17(5):1299–1306, 2021.

[8] J De Vicente, DJ Klingenberg, and R Hidalgo-Alvarez. Magnetorheological fluids: a review. *Soft Matter*, 7(8):3701–3710, 2011.

[9] Z Deng, X Wei, X Li, S Zhao, and S Zhu. Design and multi-objective optimization of magnetorheological damper considering vehicle riding comfort and operation stability. *Journal of Intelligent Material Systems and Structures*, 33(9):1215–1228, 2022.

[10] Z Strecker, F Jeniš, M Kubík, O Macháček, and SB Choi. Novel approaches to the design of an ultra-fast magnetorheological valve for semi-active control. *Materials*, 14(10):2500, 2021.

[11] J Gołdasz and B Sapiński. *Insight into magnetorheological shock absorbers*. Springer, 2015.

[12] Z Deng, Q Cai, L YunQiang, H Wei, Q Yang, and S Dong. Magnetic circuit design and optimisation of magnetorheological mount with tapered channel under the flow mode. *Journal of Intelligent Material Systems and Structures*, 32(14):1614–1623, 2021.

[13] M Elahinia, C Ciocanel, S Wang, et al. MR-and ER-based semiactive engine mounts: a review. *Smart Materials Research*, 2013, 2013.

[14] BF Spencer Jr and S Nagarajaiah. State of the art of structural control. *Journal of Structural Engineering*, 129(7):845–856, 2003.

[15] X Ruan, S Xuan, J Zhao, H Bian, and X Gong. Mechanical performance of a novel magnetorheological fluid damper based on squeeze-valve bi-mode of MRF. *Smart Materials and Structures*, 29(5):055018, 2020.

[16] MA Fernández and JY Chang. A study of factors affecting torque transmission in permanent magnet-based magnetorheological fluid clutch. *Smart Materials and Structures*, 30(6):065024, 2021.

[17] H Wang and Ch Bi. Study of a magnetorheological brake under compression-shear mode. *Smart Materials and Structures*, 29(1):017001, 2019.

[18] B Sapiński and J Gołdasz. Development and performance evaluation of an MR squeeze-mode damper. *Smart Materials and Structures*, 24(11):115007, 2015.

[19] Q Liu, GD Bai, ZH Liu, XX Bai, H Du, P Chen, and LJ Qian. Magnetorheological semi-active mount system for engines: Prototyping and testing. *Proceedings of the Institution of Mechanical Engineers, Part D: Journal of Automobile Engineering*, 234(13):3081–3094, 2020.

[20] JD Carlson, F Goncalves, D Catanzarite, and D Dobbs. Controllable magnetorheological fluid valve, devices, and methods, March 13 2008. US Patent App. 11/844,548.

[21] FD Goncalves and JD Carlson. An alternate operation mode for MR fluids—magnetic gradient pinch. In *Journal of Physics: Conference Series*, volume 149, page 012050. IOP Publishing, 2009.

[22] TH Lee, BH Kang, and SB Choi. A quasi-static model for the pinch mode analysis of a magnetorheological fluid flow with an experimental validation. *Mechanical Systems and Signal Processing*, 134:106308, 2019.

[23] J Gołdasz and B Sapiński. Magnetostatic analysis of a pinch mode magnetorheological valve. *acta mechanica et automatica*, 11(3), 2017.

[24] J Gołdasz, K Kluszczyński, and B Sapiński. Fluid flow pinched by near-wall Bingham plastic zones: simulation study. In *2018 19th International Conference on Research and Education in Mechatronics (REM)*, pages 48–51. IEEE, 2018.

[25] M Kubík, D Pavlíček, O Macháček, Z Strecker, and J Roupec. A magnetorheological fluid shaft seal with low friction torque. *Smart Materials and Structures*, 28(4):047002, 2019.

[26] T Xuan, J Li, B Li, and W Fan. Effects of the non-uniform magnetic field on the shear stress and the microstructure of magnetorheological fluid. *Journal of Magnetism and Magnetic Materials*, 535:168066, 2021.

[27] MR Jolly, JW Bender, and JD Carlson. Properties and applications of commercial magnetorheological fluids. *Journal of Intelligent Material Systems and Structures*, 10(1):5–13, 1999.

[28] L Rodríguez-Arco, P Kuzhir, MT López-López, G Bossis, and JDG Durán. Instabilities of a pressure-driven flow of magnetorheological fluids. *Journal of Rheology*, 57(4):1121–1146, 2013.

[29] A Lange. Kelvin force in a layer of magnetic fluid. *arXiv preprint cond-mat/0204196*, 2002.

[30] LMA Monzon and JMD Coey. Magnetic fields in electrochemistry: The Kelvin force. A mini-review. *Electrochemistry Communications*, 42:42–45, 2014.